in the magnetic interaction, as well as a possible first-order phase transition. Any of the three effects or a combination of them can explain the QS(T) anomaly below T_N; however, there are not enough experimental data available at present time for a meaningful discussion of this problem.[21]

[21] A still unexplored mystery of this phase transition is the vanishing magnetic field at the iron nucleus below T_N. The discussions of the "residual" field in Refs. 5 and 15 are based on an observed line broadening below T_N. The results reported in Ref. 3 show evidence for strong thermal hysteresis. In the experiment shown in Fig. 1 the spectra at 10 K showed a symmetric doublet, the linewidth of which reduced from an initial value of 1.2 to 0.4 mm/sec after about 8 h. In the following warmup the linewidth reduced continuously to 0.27 mm/sec at room temperature with no significant change at T_N. Unlike Ref. 15, the spectrum was clean of traces of the monohydrate, while in the spectra shown in Ref. 5 such traces would not have been resolved.

The purpose of the present work was to reaffirm the conclusion of Axtmann *et al.*[1–3] that there is a strong radial expansion of the 3*d* electronic wave functions in solid ferrous compounds due to covalency effects. We have demonstrated that Mössbauer QS(T) data are too simple to allow for a unique determination of crystal field parameters. The present results are consistent with the traditional concepts of covalency in the halides as well as with the Ising model for the magnetic behavior at low temperatures.

We would like to express our appreciation to J. W. Hurley for using his experimental results. The work made use of computer facilities supported in part by the National Science Foundation, under Grants Nos. NSF-GJ-34 and NSF-GU-3157.

PHYSICAL REVIEW VOLUME 188, NUMBER 2 10 DECEMBER 1969

Photoemission Studies of the Alkali Metals. I. Sodium and Potassium*

NEVILLE V. SMITH† AND WILLIAM E. SPICER
Stanford University, Stanford, California 94305
(Received 14 August 1969)

Measurements have been made of the photoelectric yield and the photoelectron energy distribution curves (EDC's) on Na and K in the photon energy range 2.3–11.6 eV. The samples were thick films prepared by evaporation onto various substrates in a specially constructed ultrahigh vacuum chamber. The results are interpreted in terms of a model which assumes that each of the three stages of the photoemission process–optical excitation of electrons, transport to the surface and escape across the surface—may be treated independently. The most noteworthy feature of the frequency dependence of the photoelectric yield, expressed in electrons per incident photon, is a sharp drop on passing through the plasma frequency. It is shown that this may be understood in terms of the rapid variations of the optical constants in this region. The EDC's are characterized by a pronounced peak at the high-energy edge which is identified as arising from primary or unscattered electrons. Its width is found to increase with increasing photon energy, an effect which can be understood in terms of the direct (or **k**-conserving) nature of the optical transitions. The simple theory of direct transitions in a nearly free-electron metal is expounded, and the form of the EDC is derived. It is predicted that the optically excited electrons should originate from initial states which are distributed uniformly between a maximum energy equal to the Fermi energy E_F and a minimum energy $E_{\min}$ which varies quadratically with photon energy. In the experimental range, the width $E_F - E_{\min}$ is predicted to increase with photon energy, in agreement with the observed behavior. However, the predicted shape of the EDC's is rectangular, whereas the observed shape is more triangular. The other main feature of the EDC's is an abundance of electrons at energies below the leading peak. These are identified as electrons which have undergone an inelastic scattering due to electron-electron interactions before emerging from the metal. This region of the EDC may be regarded as a kind of characteristic energy-loss spectrum. Na shows a single, rather wide low-energy peak in this region. K shows a narrower low-energy peak and a broad intermediate bump identified as a plasmon energy loss. This intermediate bump has been seen also in preliminary work on Rb and Cs, and is found to become more pronounced and closer to the leading peak. The systematic trends therefore support the plasmon interpretation. The energy separation of the peaks is more consistent with a surface rather than a volume plasmon loss. The structure identified as plasmon energy loss is, however, superimposed on a large background, which is attributed to energy loss by pair creation. Rough estimates of the relative proportions indicate that pair creation dominates plasmon creation as the main scattering mechanism.

I. INTRODUCTION

THE alkali metals form an ideal system for the fundamental investigation of photoemission. Their band structures are believed to be simple, so that the predictions of conventional theory may be easily worked out and tested. Scattering due to electron-electron interactions plays an important part in

* Work supported by the Advanced Research Projects Agency through the Center for Materials Research at Stanford University and by the National Science Foundation.

† Present address: Bell Telephone Laboratories, Murray Hill, N. J. 07971.

the photoemission process, and most of the theoretical work on the electron-electron interaction is directly applicable only to simple metals. The alkali metals also have small work functions, small Fermi energies, and small plasma frequencies. This brings all the interesting effects well within the present accessible energy range of optical experiments. In this paper, we describe some measurements of the photoelectric yield and electron energy distributions from Na and K. We discuss the extent to which they can be reconciled with our present ideas on the nature of optical absorption, electron-electron scattering, and the photoemission process in general.

There have been many previous investigations of the photoelectric effect in the alkali metals. Much of the early work was directed towards answering two very basic questions. First, what is the relationship between the photoelectric effect and the conventional optical constants? Second, is photoemission a volume or a surface effect? The answer to the first question has been provided by Ives, Briggs, and Fry in a series of experiments[1] on alkali metal films deposited on various substrates. They were able to show that the previously mysterious dependence of the photoelectric yield on polarization and angle of incidence of the incoming light could be understood quite naturally in terms of Maxwell's equations and a knowledge of the optical constants of the alkali metal and the substrate. Their work demonstrates the need for reliable values of the optical constants and appears to have provided the stimulus for their own well-known measurements of the optical constants.[2] Our own measurements of the yield at normal incidence are presented in Sec. III and are interpreted in much the same spirit. We have used here the new values for the optical constants obtained recently by Smith.[3]

Mayer and Thomas[4] have performed experiments similar to those of Ives and Briggs. They have measured the reflectivity, transmission, and photoelectric yield simultaneously on thin-film samples of K deposited on quartz. They observed a very close correspondence between the absorption of the film and the photoelectric yield. Mayer and Thomas also give a detailed and closely argued case for why photoemission should be considered a volume rather than a surface effect. The correlation between the photoelectric current and the bulk optical behavior is, of course, very suggestive of a volume effect. However, a most convincing experimental demonstration in support of the volume nature of photoemission has been provided by Thomas,[5] and extended by Piepenbring.[6] Their experiments consist of depositing Na or K onto quartz substrates and measuring the photoelectric yield as a functions of thickness. At the longest wavelengths, several hundred angstroms of metal are required before the photocurrent reaches its saturation value, clearly demonstrating the volume nature of the process. It was found, however, that the average escape depth deduced from these experiments was a rapidly decreasing function of frequency. The importance of electron-electron interactions in cutting down the mean free path of excited electrons was quickly recognized. Electrons which are excited to states high above the Fermi level have an increasingly short lifetime due to decay via the electron-electron interaction. There are two basic loss mechanisms, decay by plasmon creation and decay by pair creation. Thomas[5] made an important contribution here by deriving theoretically an expression for the mean free path due to plasmon creation. More recent theoretical work by Quinn[7] indicates that pair creation may be equally important, and we will discuss this in more detail in Sec. VI.

Further confirmation of the importance of scattering due to electron-electron interactions has been provided by Dickey[8] and by Methfessel[9] in their measurements of the energy distribution curves (EDC's) of photoemitted electrons from Na, K, and Cs. They find an abundance of electrons in the EDC's at energies too low to be primary (i.e., unscattered) electrons. These are presumably electrons which have undergone an inelastic scattering event before escaping from the metal. The maximum photon energy in this earlier work was set at 6–7 eV by the transmission limit of quartz optics. Perhaps the most important advance we have made in the present work is in extending the measurement of EDC's to photon energies up to 11.2 eV. These results are presented in Sec. IV and it may be seen that we have been able to uncover much more information on the relative contributions of scattered and unscattered electrons. For example, K has a free-electron Fermi energy of 2.1 eV and a work function of 2.3 eV. At $\hbar\omega = 11.2$ eV the electrons which emerge from the metal without scattering must have kinetic energies in the range 6.8–8.9 eV. The volume and surface plasmon energies[10] in K are, respectively, 3.7 and 2.5 eV. This means that electrons which have suffered an inelastic scattering through plasmon creation should emerge from the metal with kinetic energies in the 3–6-eV region. One of our aims was to search this energy region for evidence of such scattering processes and was made possible by the high photon energies available

[1] H. E. Ives, Phys. Rev. **38**, 1209 (1931); H. E. Ives and H. B. Briggs, *ibid.* **38**, 1447 (1932); **40**, 802 (1932); H. E. Ives, H. B. Briggs, and T. C. Fry, J. Opt. Soc. Am. **23**, 73 (1933).
[2] H. E. Ives and H. B. Briggs, J. Opt. Soc. Am. **26**, 238 (1936); **27**, 181 (1937).
[3] N. V. Smith, Phys. Rev. Letters **21**, 96 (1968); Phys. Rev. **183**, 634 (1969).
[4] H. Mayer and H. Thomas, Z. Physik **147**, 419 (1957).
[5] H. Thomas, Z. Physik **147**, 395 (1957).
[6] F. J. Piepenbring, in *Proceedings of the International Colloquium on the Optical Properties and Electronic Structure of Metals and Alloys* (North-Holland Publishing Co., Amsterdam, 1966), p. 316.
[7] J. J. Quinn, Phys. Rev. **126**, 1453 (1962).
[8] J. Dickey, Phys. Rev. **81**, 612 (1951).
[9] S. Methfessel, Z. Physik **147**, 442 (1957).
[10] C. Kunz, Z. Physik **196**, 311 (1966).

to us. It will be seen that there is indeed some structure in this energy region.

The prevailing view of the photoemission process deduced from the previous work on alkalis and the parallel work on other materials[11] may be summarized as follows. The process is envisaged in three steps. First, the electrons are optically excited within the material to a characteristic depth of α^{-1}, where α is the optical-absorption coefficient related to the conventional optical constants. Second, some of these electrons reach the surface. Third, some of these escape across the surface into the vacuum. Before reaching the surface, however, the electrons may suffer an inelastic scattering, and the electron-electron interaction is believed to be the dominant scattering mechanism. The probability of scattering is usually expressed in terms of an energy-dependent mean free path $l(E)$. The transport theories by Berglund and Spicer[12] and by Kane[13] show that the probability of arrival at the surface contains the factor $\alpha l/(1+\alpha l)$. Electrons which have undergone an inelastic scattering event may also arrive at the surface and, if they are still sufficiently energetic to surmount the potential barrier, may escape across it. The energy distribution of these slower secondary electrons may be thought of as an energy-loss spectrum in close analogy with the characteristic energy-loss spectra[14] which are measured for fast electrons.

The three-step picture of photoemission outlined above may not be strictly correct in that it treats each of the steps independently. Sutton and Hopfield[15] have developed a quantum-mechanical formalism in which the optical excitation, the scattering, and the transfer across the surface are associated in a one-step process. The involvement of the scattering as an integral part of the optical excitation event has also been considered by Nesbet and Grant[16] in a discussion of the "anomalous" peaks and nondirect behavior which characterize some materials. In a more quantitative approach, Hedin, Lundqvist, and Lundqvist[17] show that the effects of scattering due to plasmon creation and pair creation can be incorporated into the electronic states prior to optical excitation. They find that the energy distribution of electrons has an appreciable low-lying peak which should be observable in photoemission. From a purely experimental standpoint, these various approaches bear some resemblance to the simple three-step model. They all seem to predict that a peak in the energy distribution of unscattered electrons should be accompanied by a secondary peak shifted down by the plasmon energy.

Other many-body effects have been proposed for the alkali metals. Phillips[18] suggests that the data of Dickey may be better understood in terms of a collective resonance of the electron gas. Hopfield[19] has applied his ideas of dynamic screening to numerical calculations of the photoemission EDC's from potassium. A discussion of the precise relationships and relative merits of the various many-body theories mentioned above is beyond the scope of this paper. The interpretation of our data will be presented solely in terms of the conceptually simpler three-step model. Indeed, our intention is to see how far we can get with conventional theory before invoking anything more sophisticated. At the same time, we hope that our experiments will stimulate deeper quantitative theories such as the elegant work by Hedin *et al.*

Even within the three-step model, the nature of the optical excitation can present problems. Although photoemission is regarded as a volume process, it has been found that in some materials it is difficult to reconcile the experiments with the well-known **k**-selection rule which operates for direct transitions. A nondirect model in which the **k**-selection rule is abandoned has been found to work quite successfully for these materials. However, nondirect transitions, when they occur, appear to be associated with states whose wave functions are tightly bound.[20] The electrons in the alkali metals are believed to be very free, and so we may expect direct transitions to be more appropriate. The predictions of direct transitions in a simple nearly free-electron model are expounded in Sec. V and are shown to account reasonably well for some of the systematic trends of the primary electrons.

II. EXPERIMENTAL METHOD

The specimens used in these experiments were thick films prepared by evaporation in an ultrahigh vacuum system illustrated schematically in Fig. 1. The system consists of a stainless-steel chamber and is evacuated to pressures of typically 3×10^{-11} Torr by means of a Varian Noble Vac-ion combination pump. The substrate, which was made of mechanically polished copper or silver, could be moved between the two alternative positions shown in Fig. 1 by means of a linear motion and bellows assembly. In the upper position, the substrate stands opposite a lithium fluoride window which admits light from the monochromator. The substrate here is inside a cylindrical copper collector can to which retarding voltages can be applied during the course of photoemission experiments.

[11] See A. H. Sommer and W. E. Spicer, in *Photoelectronic Materials and Devices* (D. Van Nostrand Co., Inc., Princeton, N. J., 1965), and references therein.

[12] C. N. Berglund and W. E. Spicer, Phys. Rev. **136**, A1030 (1964).

[13] E. O. Kane, Phys. Rev. **147**, 335 (1966).

[14] D. Pines, *Elementary Excitations in Solids* (W. A. Benjamin, Inc., New York, 1964), p. 182.

[15] L. Sutton and J. J. Hopfield (private communication).

[16] R. K. Nesbet and P. M. Grant, Phys. Rev. Letters **19**, 222 (1967).

[17] L. Hedin, B. J. Lundqvist, and S. Lundqvist, Solid State Commun. **5**, 237 (1967).

[18] J. C. Phillips, Phys. Rev. **137**, A1835 (1965).

[19] J. J. Hopfield, Phys. Rev. **139**, A419 (1965).

[20] W. E. Spicer, Phys. Rev. **154**, 385 (1967).

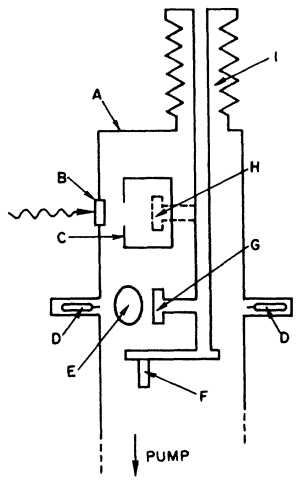

FIG. 1. Schematic diagram of sample chamber: A, stainless-steel chamber wall; B, lithium fluoride window; C, cylindrical collector electrode; D, ampules containing alkali metal sealed under vacuum; E, ellipsometry windows; F, fused quartz prism used in some of the ellipsometry experiments; G, sample substrate in evaporation position; H, alternative position of substrate during actual photoemission measurements; I, linear motion bellows assembly for moving substrate between alternative positions.

In the lower position, the substrate stands opposite the evaporation source. The chamber was provided with two fused quartz windows at this same lower level to enable ellipsometry experiments to be performed on the sample. In some experimental runs, a fused quartz prism was attached at the lower end of the linear motion. By positioning this at the level of the evaporation sources, it was possible to deposit metal on one or both sides of the prism and then perform ellipsometry

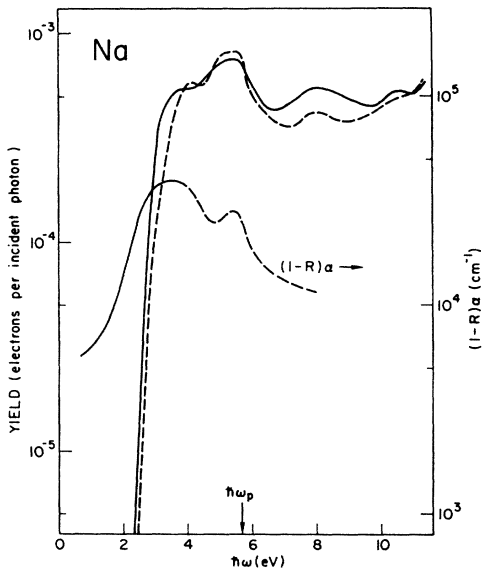

FIG. 2. Photoelectric yield for Na plotted against frequency. The full curve was obtained on a diffuse sample, and broken curve on a shiny sample. The frequency variation of $(1-R)\alpha$ is also shown. The plasma frequency $\hbar\omega_p$ occurs at 5.7 eV.

experiments *in situ* at the quartz-metal interfaces. These ellipsometry experiments have been presented in detail elsewhere,[3] and only the results will be mentioned here.

The samples were originally sealed under vacuum in glass ampules. These in turn were placed inside soft copper tubes which projected from the main body of the vacuum chamber as shown in Fig. 1. The procedure in a typical run was as follows. Keeping the ampules intact, the system was pumped and baked in a fairly standard fashion. Pressures low on the 10^{-11} Torr scale were routinely obtained. The ampule was then broken open by crushing the soft copper tube. The subsequent burst of gas was pumped away. The pressure would return to the 10^{-11} Torr scale by the following day. The samples were then evaporated onto the substrate by means of a heater wrapped round the tube. The pressure, measured by a ionization gauge out of line of sight of the source, rose during the evaporations to about 5×10^{-9} Torr in the Na experiments and to about 2×10^{-8} Torr in the K experiments. Deposition rates were slow, taking typically 1 h to deposit a large thickness. The specimens obtained were usually diffusely reflecting. Shiny specimens could be obtained by cooling the substrate with liquid nitrogen during deposition.

The alkali-metal-covered substrate was then raised to the upper position and the photoemission measurements taken. The energy distributions of photoemitted electrons were measured by an ac modulated-retarding-potential method due to Eden[21] and similar to that described by Spicer and Berglund.[22] The photoelectric yield was determined by measuring the photocurrent emitted by the sample when a relatively large accelerating voltage (+45 V) was applied to the collector can. This current was then converted to a quantum yield by comparing against the photocurrent of a Cs_3Sb photodiode calibrated in this laboratory by Koyama. A correction was made for the transmission efficiency of the lithium flouride window of the chamber.

The substrate was provided with a heater so that it was possible to remove the sample by evaporation. Further samples could then be prepared and tests of reproducibility made. The photoemission properties of the substrate material were checked at the beginning of the measurements. Copper and silver have very characteristic energy distributions[23] due to the presence of *d* electrons. In some experiments, the alkali metal was deposited in successive small thicknesses. It was then possible to observe the energy distribution characteristic of the substrate disappear and be progressively replaced by the one characteristic of the alkali metal. When no further change took place, the

[21] R. C. Eden (to be published).
[22] W. E. Spicer and C. N. Berglund, Rev. Sci. Instr. **35**, 1665 (1964).
[23] C. N. Berglund and W. E. Spicer, Phys. Rev. **136**, A1044 (1964); W. F. Krolikowski and W. E. Spicer, *ibid.* (to be published).

evaporations were discontinued. The final results on the alkali metal were found to be independent of whether the substrate was copper or silver.

One difficulty encountered seems to be peculiar to these experiments and due to the high volatility of sodium and potassium. Monolayers of alkali metal were readily accumulated on all the internal parts of the chamber, lowering their work functions and increasing their photoelectric yield. Photoelectrons emitted from these surfaces were able to find their way to the sample and cause a reverse photocurrent, sometimes comparable in magnitude to the current from the sample itself. This was accompanied by a distortion of the low-energy end of the measured energy distributions. The distortion and reverse current could be temporarily removed by heating the parts of the chamber in the vicinity of the window to disperse the condensed material. During the course of an experimental run, which typically lasted several days, a considerable amount of the alkali metal was released into the chamber. It was found that the pressure gradually rose over this period and finally leveled at a value close to the vapor pressure of the metal at room temperature.

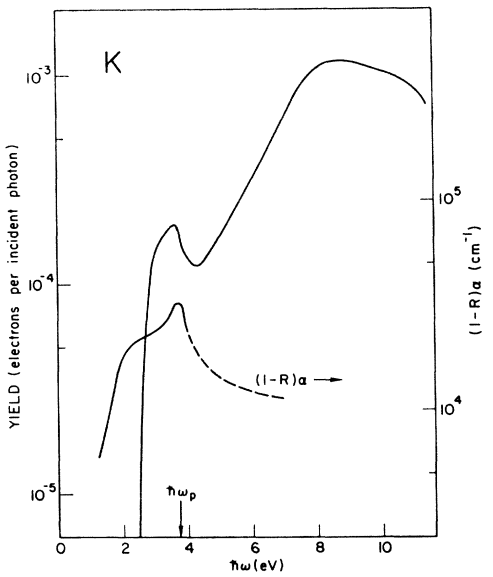

FIG. 3. Photoelectric yield for K plotted against frequency. The curve for $(1-R)/\alpha$ is shown. The plasma frequency $\hbar\omega_p$ occurs at 3.8 eV.

III. PHOTOELECTRIC YIELD: RESULTS AND DISCUSSION

The measured photoelectric yield $Y_{\rm inc}$ expressed as the number of photoemitted electrons per incident photon is plotted against photon energy $\hbar\omega$ in Figs. 2 and 3. First, we observe that the yields are very small, being rarely greater than 10^{-3} electrons per incident photon. Fowler plots[24] of $Y_{\rm inc}^{1/2}$ against $\hbar\omega$ were found to be fairly linear within about 1 eV of threshold, and the values of the work function $e\varphi$, deduced from the intercepts on the $\hbar\omega$ axis, were 2.3±0.1 eV for Na and 2.3±0.1 eV for K. These are in agreement with values obtained by other workers.[25]

For sodium, results are shown in Fig. 2 for both shiny and diffusely reflecting surfaces. Over most of the range, the shiny surface has the lower yield, an effect which has been observed previously by Dickey,[8] and which is explained by the fact that the yield is known to increase with increasing angle of incidence. A diffuse surface consists of facets for which there is a wide range of angles of incidence, whereas a shiny surface presents one face normal to the beam.

An interesting feature shown by all samples of both metals was a pronounced fall in $Y_{\rm inc}$ on passing through the plasma frequency. In the spirit of earlier work, such as that by Ives and Briggs,[1] we will now investigate the extent to which this behavior can be understood in terms of the optical constants. Since our investigation is hindered by our incomplete knowledge of the optical constants over the whole frequency range, it will become necessary to make some plausible extrapolations.

We first relate the yield per *incident* photon to the yield per *absorbed* photon $Y_{\rm abs}$ by means of the reflectance R:

$$Y_{\rm inc}=(1-R)Y_{\rm abs}. \tag{3.1}$$

The quantity $(1-R)$ is sometimes called the absorptance. $Y_{\rm abs}$ is composed of contributions from all electrons whose energy is sufficient to overcome the work function. An electron which has been excited to an energy E must reach the surface before it can escape and be detected as a photoelectron. The transport theories of Berglund and Spicer[12] and Kane[13] show that the number of electrons of energy E reaching the surface contains the arrival factor:

$$P_{\rm arr}(E)=\alpha(\omega)l(E)/[1+\alpha(\omega)l(E)], \tag{3.2}$$

where $l(E)$ is an energy-dependent mean free path, $\alpha(\omega)$ is the optical absorption coefficient, and α^{-1} is a measure of the penetration depth of the electromagnetic field. That the mean free path $l(E)$ is a rapidly decreasing function of energy implies two limiting cases for Eq. (3.2). At low frequencies (i.e., just above threshold) the excited electrons have relatively low energies, for which $\alpha l\gtrsim 1$. In this case $P_{\rm arr}\simeq 1$ for all electrons. Provided that the optical excitation probabilities do not vary wildly, we may then expect much of the frequency dependence of $Y_{\rm inc}$, particularly structure in the frequency dependence, to be contained in the factor $(1-R)$ in Eq. (3.1).

However, as we proceed to higher frequencies, electrons will be excited to states for which the mean free

[24] R. H. Fowler, Phys. Rev. 38, 45 (1931).
[25] V. S. Fomenko, in *Handbook of Thermionic Properties*, edited by G. V. Samsonov (Plenum Press, Inc., New York, 1966).

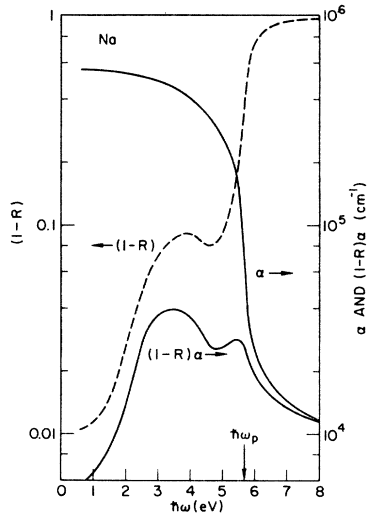

FIG. 4. Na: Frequency dependence of the absorptance $(1-R)$, the absorption coefficient α, and their product. The values above $\hbar\omega=4$ eV were obtained by an extrapolation procedure described in the text.

path is short. The condition $\alpha l \ll 1$ will then apply for the majority of the excited electrons. In this second limiting case, we have $P_{\text{arr}} \simeq \alpha l$. Therefore, the probability of a high-energy electron reaching the surface and eventually being detected as a photoelectron contains the additional factor α. If we assume that l and the optical excitation probabilities are smoothly varying, we now expect any structure in the frequency dependence of Y_{inc} to be contained in the factor $(1-R)\alpha$. This simple picture, therefore, implies two regions of behavior; a low-frequency region in which Y_{inc} is correlated strongly with $(1-R)$, passing to a high-frequency region where Y_{inc} depends more on $(1-R)\alpha$.[26] Estimates of α and l indicate that the latter behavior will be appropriate over most of our frequency range. Testing these predictions presented some difficulty since the optical constants are not completely known over the whole frequency range. We therefore attempted the extrapolation described below.

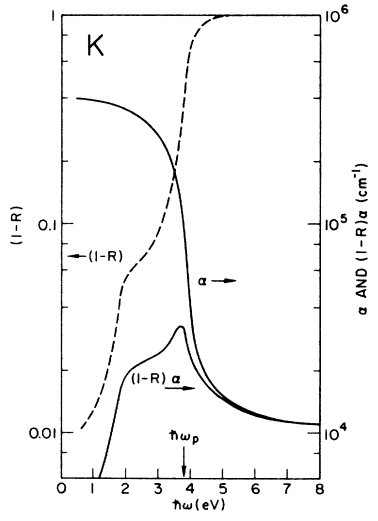

FIG. 5. K: Frequency dependence of the absorptance $(1-R)$, the absorption coefficient α, and their product. The values above $\hbar\omega=4$ eV were obtained by an extrapolation procedure described in the text.

Smith[3] has measured both ϵ_1 and ϵ_2, the real and imaginary parts of the dielectric constant, for both Na and K from $\hbar\omega=0.5$–4.0 eV. Above 4 eV Sutherland *et al.*[27] have measured ϵ_1; their values match quite well those of Smith, below 4 eV. We therefore have a complete picture of ϵ_1 over the whole range. Since there are, however, no really reliable measurements of ϵ_2 above 4 eV, we made a smooth extrapolation of Smith's values for the optical conductivity $\sigma(\omega)$ $(=\omega\epsilon_2/4\pi)$ into this region. For potassium, $\sigma(\omega)$ was simply set equal to the constant value 0.25×10^{14} sec^{-1} above 4 eV. For sodium, $\sigma(\omega)$ was put equal to the constant value 0.20×10^{14} sec^{-1} above $\hbar\omega=5$ eV and was joined smoothly to the experimental data at 4 eV. The value of 0.20×10^{14} sec^{-1} was chosen as reasonably consistent with several scattered experimental values of σ obtained in this range by Ives and Briggs[2] and by Sutherland *et al.*[28] Having thus obtained smooth curves for ϵ_1 and σ over a wide frequency range, they were then converted to a complex refractive index $n-ik$, and the values of R and α were calculated from the standard formulas

$$R=[(n-1)^2+k^2]/[(n+1)^2+k^2],$$
$$\alpha=4\pi k/\lambda,$$

where λ is the free-space wavelength. The curves obtained for $(1-R)$, α, and $(1-R)\alpha$ are shown in Figs. 4 and 5. Since our extrapolations are somewhat arbitrary, the actual numerical values should not be taken too seriously, although it was found that all plausible extrapolations showed the same qualitative features. It is found that the quantity $(1-R)\alpha$ invariably exhibits a peak just below the plasma frequency. (The plasma frequency is defined here as the frequency at which the experimental ϵ_1 passes through zero.) Although ϵ_1

[26] These arguments apply to bulk samples. There is a third case to consider when the samples are thin films. If the thickness of the film is much less than α^{-1}, then the electromagnetic field permeates the whole sample and the dependence of the arrival probability on α drops out. Y_{inc} will then be expected to correlate with the absorptance alone over the whole frequency range. However, it must be remembered that such samples will be transparent and that the absorptance is no longer $(1-R)$ but is now equal to $(1-R-T)$, where T is the transmittance. Such a correlation has been observed by Mayer and Thomas (Ref. 4) on thin films of K. Their work is therefore not inconsistent with the picture outlined above. Our argument ignores the frequency dependence of the escape probability which must tend to zero as $\hbar\omega$ approaches threshold $e\varphi$. Our concern here is primarily with structure in the frequency dependence of Y_{inc}.

[27] J. C. Sutherland, E. T. Arakawa, and R. N. Hamm, J. Opt. Soc. Am. **57**, 645 (1967); J. C. Sutherland and E. T. Arakawa, *ibid.* **58**, 1080 (1968).

[28] J. C. Sutherland, Ph.D. thesis (Georgia Institute of Technology, 1967), Oak Ridge National Laboratory Report No. ORNL-TM-1776 (unpublished).

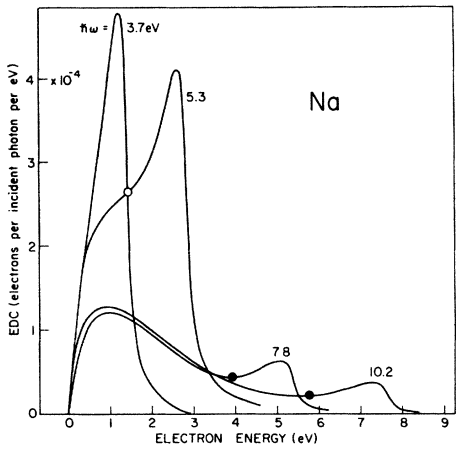

FIG. 6. Na: Photoelectron energy distributions normalized to the yield per incident photon and plotted against E, the kinetic energy in vacuum, for several photon energies.

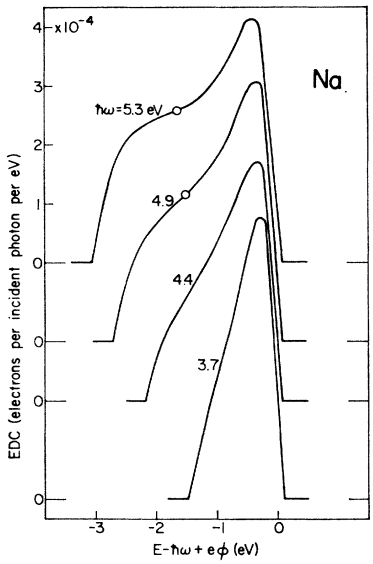

FIG. 7. Na: Photoelectron energy distributions for low photon energies. Curves are normalized to the yield per incident photon, and are plotted against initial energy $E-\hbar\omega+e\varphi$.

and σ are varying very slowly in this region, it can be seen that $1-R$ is rapidly increasing and α is rapidly decreasing. In the product $(1-R)\alpha$ the two factors tend to compensate, except for the peaking effect mentioned above. We therefore offer this effect in explanation of the peaks observed in the experimental yield. Figures 2 and 3 compare Y_{ine} and the calculated $(1-R)\alpha$. It is seen that the agreement is quite good for the peak just below the plasma frequency and is reasonably good for the structure at even lower frequencies which can be traced to interband transitions. Explanation of the structure at higher frequencies must await a better knowledge of the optical constants.

An alternative explanation for the drop in yield is that it is due to a sudden drop in the mean free path $l(E)$ for electrons which are excited to energies in excess of $E_F+\hbar\omega_p$, where E_F and $\hbar\omega_p$ are, respectively, the Fermi and volume plasmon energies. Such electrons are able to decay by the additional process of plasmon creation, and Thomas[5] has argued that the mean free path should vary very strongly at this energy. In later sections of this paper we will argue that the variation of the mean free path may not be so dramatic. We point out at this stage that a sudden drop in $l(E)$ is not necessary to explain the yield data. The drop in yield on passing through the plasma frequency appears to follow quite naturally from the frequency dependence of the optical constants.

IV. RESULTS FOR ENERGY DISTRIBUTIONS

A. Sodium

The measured EDC's of photoemitted electrons from Na are shown for four widely spaced photon energies in Fig. 6. Each curve has been normalized, so that the area under it is proportional to the yield per incident photon. The sharp decrease in the height of the leading edge between the curves for $\hbar\omega=5.3$ and 7.8 eV can be traced to the pronounced drop in the yield on passing through the plasma frequency discussed in Sec. III.

As the photon energy is increased, a peak begins to emerge at the high-energy end of the EDC. The open circle on the EDC for $\hbar\omega=5.3$ eV represents the estimated position of the point of inflection. At the higher photon energies, the high-energy peak is separated from the low-energy end of the EDC by a definite valley. The full circles on these curves represent the estimated position of the minimum in the valley. In

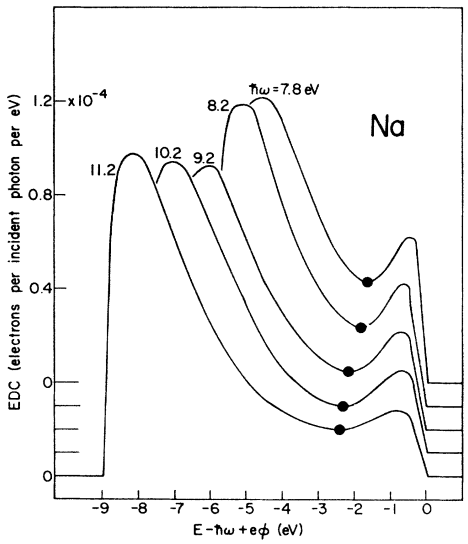

FIG. 8. Na: Photoelectron energy distributions for high photon energies. Curves are normalized to the yield per incident photon, and are plotted agains initial state energy $E-\hbar\omega+e\varphi$.

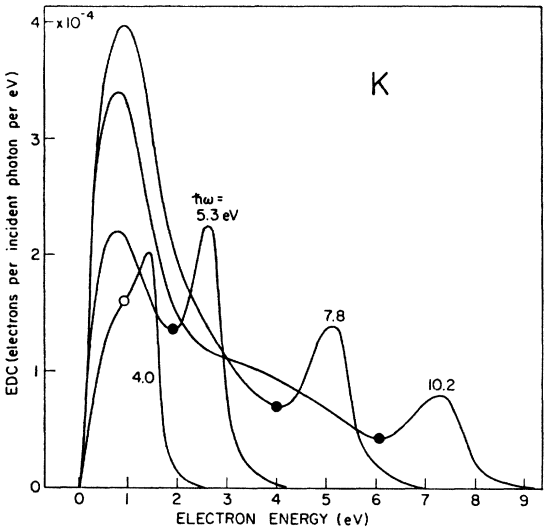

FIG. 9. K: Photoelectron energy distributions normalized to the yield per incident photon and plotted against E, the kinetic energy in vacuum, for several photon energies.

what follows, the full and open circles will be taken to represent the low-energy demarcation of the peak. This choice is somewhat arbitrary, but will be found to be helpful when we come to examine the systematics of the peak.

Figures 7 and 8 show the EDC's for low and high photon energies, respectively. Here we plot the EDC's against $E-\hbar\omega+e\varphi$, where E is the kinetic energy in vacuum, $\hbar\omega$ is the photon energy, and $e\varphi$ is the work function. This choice of scale refers the electrons to their initial-state energies and places the zero of energy at the Fermi level. The full and open circles again represent valley minima and inflections. It can be seen that the width of the leading peak, defined here as the distance between the valley (or inflection) and the leading edge, tends to increase with increasing photon energy.

The leading peak, however, constitutes only a small proportion of the total electrons observed. The EDC's show a low-energy peak which becomes relatively larger with increasing $\hbar\omega$. This abundance of low-energy electrons has been noted previously by Dickey[8] in Na, and is a well-known feature of other materials. Since the Fermi energy for Na is about 3.2 eV, we might naively expect all the photoemitted electrons to appear within 3.2 eV of the leading edge. However, an electron which has been optically excited in the bulk of the sample has a strong probability of suffering an inelastic scattering before it escapes into the vacuum. The scattering mechanisms are believed to be due to interactions with other electrons and possibly with the surface. It is therefore tempting to identify the high-energy peak in the EDC's with unscattered electrons, and the lower-energy peak with scattered electrons. Using a simple scattering theory, Berglund and Spicer[12] have shown that a low-energy peak is expected having much the same shape as that which is observed.

B. Potassium

The measured EDC's for K, normalized to the yield per incident photon, are shown in Figs. 9–11. The behavior is similar to that for Na. The open and full circles again denote the positions of inflections and valley minima. As with Na, a peak is seen to emerge at the high-energy end of the EDC. The increase in width

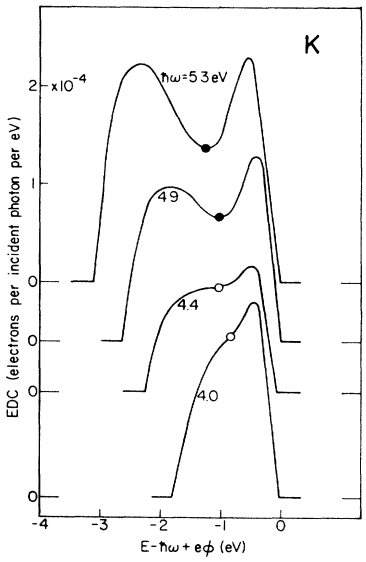

FIG. 10. K: Photoelectron energy distributions for low photon energies. Curves are normalized to the yield per incident photon, and are plotted against initial state energy $E-\hbar\omega+e\varphi$.

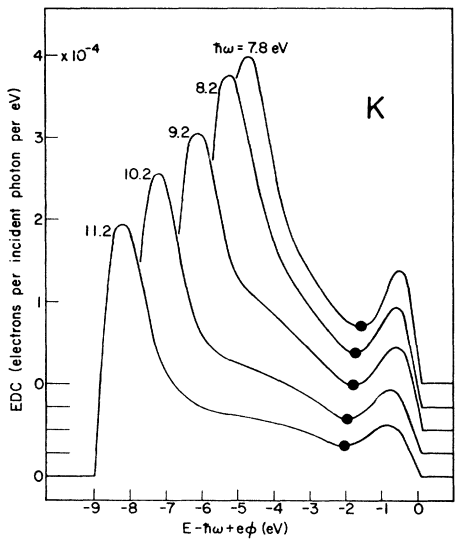

FIG. 11. K: Photoelectron energy distributions for high photon energies. Curves are normalized to the yield per incident photon, and are plotted against initial state energy $E-\hbar\omega+e\varphi$.

of this peak with increasing photon energy can be seen much more clearly in K. At the low photon energies, shown in Fig. 10, the width of the peak is about 1 eV or less. At the higher photon energies shown in Fig. 11, the peak is nearer 2 eV in width. This effect will be examined further in Sec. V.

As in Na, there is an abundance of low-energy electrons particularly for the higher photon energies, but there is one very intriguing difference. In addition to the sharp low-energy peak, the EDC's in Fig. 11 show a broad piece of intermediate structure. Its existence is presumably associated with the nature of the inelastic scattering processes and will be discussed in more detail in Sec. VI.

V. NEARLY FREE-ELECTRON MODEL

Both Na and K are regarded as good examples of the nearly free-electron metal having only small energy gaps at the Brillouin-zone boundaries. The predictions of the model for the volume photoelectric effect have been expounded by Mayer and Thomas[4] and by Methfessel,[9] and a similar treatment follows here.

A direct transition in a monovalent nearly free-electron metal is best visualized in the extended-zone scheme as illustrated in Fig. 12. An electron in an initial state of wave vector $\mathbf{k}$ and energy $E(\mathbf{k})$ absorbs a photon of energy $\hbar\omega$. To satisfy momentum conservation, the electron also suffers a Bragg reflection through the reciprocal-lattice vector $\mathbf{G}$, and arrives at the final state $\mathbf{k}+\mathbf{G}$ of energy $E(\mathbf{k}+\mathbf{G})$. Energy conservation requires that

$$E(\mathbf{k}+\mathbf{G})-E(\mathbf{k})=\hbar\omega, \tag{5.1}$$

which defines a surface in $\mathbf{k}$ space. Since the Fermi sphere of a monovalent metal lies within the first Brillouin zone, the initial and final states are fairly well removed from the zone boundaries. The deviations from the free-electron parabola in these regions are therefore small, and we may, to a good approximation, replace $E(\mathbf{k})$ and $E(\mathbf{k}+\mathbf{G})$ by their free-electron values. Equation (5.1) then becomes the plane

$$2\mathbf{k}\cdot\mathbf{G}=(2m/\hbar^2)\hbar\omega-G^2. \tag{5.2}$$

Those states whose $\mathbf{k}$ values lie on the portion of this plane inside the Fermi sphere are good candidates as the initial state in a direct optical transition at photon energy $\hbar\omega$. This defines the disk of permitted initial states illustrated in Fig. 13. Several useful results follow immediately from a consideration of the geometry of the plane and sphere shown in Fig. 13.

First, we note that at zero frequency, the plane is simply a zone boundary and therefore does not intersect the Fermi sphere. As the frequency is increased, the plane sweeps from left to right. There is a frequency at which the plane first touches the sphere, the interband threshold frequency, which is given by

$$\hbar\omega_{\rm lo}=(\hbar^2/2m)(G-2k_F)G, \tag{5.3}$$

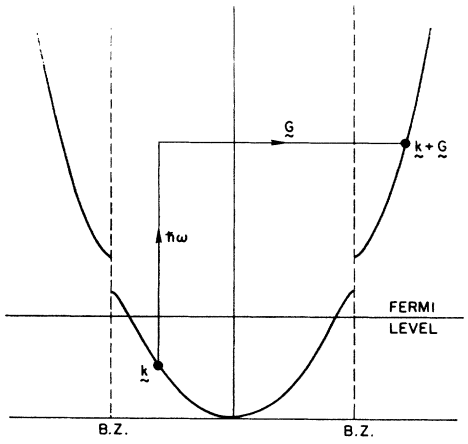

FIG. 12. Direct transition in the extended-zone scheme.

where k_F is the free-electron Fermi wave number. On increasing the frequency further, the area of the disk grows to become a maximum when the plane passes through the center of the sphere. The area then begins to diminish and finally vanishes when the plane passes out of the sphere at a frequency given by

$$\hbar\omega_{\rm hi}=(\hbar^2/2m)(G+2k_F)G. \tag{5.4}$$

Interband transitions associated with the reciprocal-lattice vector $\mathbf{G}$ are therefore only permitted between the low- and high-frequency thresholds $\omega_{\rm lo}$ and $\omega_{\rm hi}$.

Having identified the initial states, our next concern is to deduce their energy distribution. The extremal energies can be obtained immediately. The maximum initial energy corresponds to a state on the periphery of the disk shown in Fig. 13, and its energy is equal to the Fermi energy; we have

$$E_{\rm max}=E_F=(\hbar^2/2m)k_F^2. \tag{5.5}$$

The minimum initial energy corresponds to the state at the center of the disk. Since $\mathbf{k}$ is antiparallel to $\mathbf{G}$ for this state, it follows from Eq. (5.2) that its energy

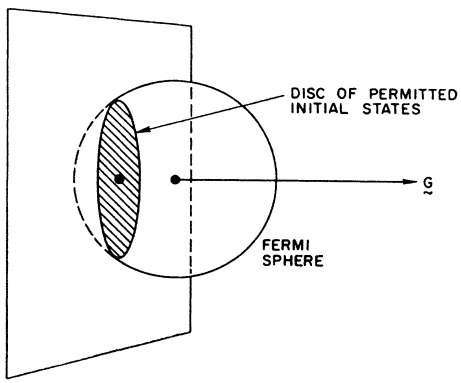

FIG. 13. Permitted initial states in direct transitions lie on the cross-hatched disk, which is the portion of the plane of constant interband energy lying inside the Fermi sphere.

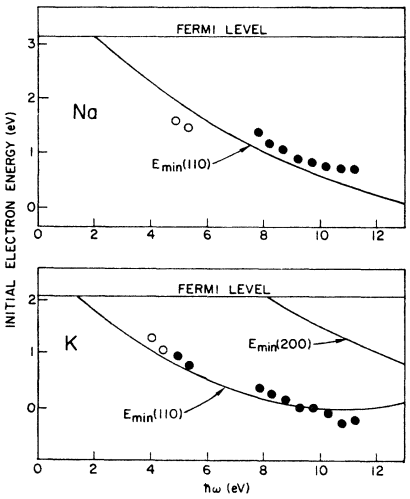

FIG. 14. Frequency variation of $E_{\min}$ for both Na and K. Smooth curves are calculated, the full and open circles represent, respectively, the position of valley minima and points of inflection such as those shown in Figs. 7, 8, 10, and 11.

is given by

$$E_{\min}=\frac{2m}{\hbar^2}\left(\frac{\hbar\omega-\hbar^2G^2/2m}{2G}\right)^2. \tag{5.6}$$

At this point it is convenient to compare these simple results with experiment. Figure 14 shows the quadratic variation of $E_{\min}$ with frequency for both Na and K. The reciprocal-lattice vector $\mathbf{G}$ was taken to be $\mathbf{G}_{110}$, associated with 110 direction. The full circles represent the positions of the valleys in the experimental energy distributions indicated in Figs. 6–11 and referred to initial-state energy. These points were plotted so that their distances below the Fermi level were equal to the distances of the estimated position of the valley below the leading edge of the energy distribution. The open circles represent the corresponding positions of the points of inflection shown also in Figs. 6–11. There is good correlation between these points and the theoretical curves for $E_{\min}$, demonstrating that the high-energy peaks in the EDC's fall within permitted range for direct transitions. K shows the best agreement. The increase in width of the peak, noted earlier, from about 1 eV at low photon energies to about 2 eV at high photon energies, is now seen to be entirely consistent with our direct transition model. The closeness of the agreement may be somewhat fortuitous, since our choice of the valley as the low-energy demarcation of the leading peak is arbitrary. However, it is worth pointing out that the results are definitely inconsistent with any simple nondirect approach. In the simple nondirect approach,[12,23] we would expect the leading peak to maintain a constant width equal to the Fermi energy; this is clearly not the case.

Pursuing the nearly free-electron model further, we may arrive at predictions for the height and shape of the leading peak. Wilson[29] and Butcher[30] show that the matrix element for an optical transition between the two states indicated in Fig. 12 is proportional to $V_G/\hbar\omega$, where V_G is the Gth Fourier component of a pseudopotential. Note that insofar as V_G may be treated as a constant, the matrix element is constant over the whole disk of permitted initial states. To obtain the energy distribution we construct two spheres of constant energy E and $E+dE$. The portion of the disk enclosed by these two surfaces is a ring of area dA:

$$dA=(2m\pi/\hbar^2)dE.$$

Note that dA, like the matrix element, is independent of E or $\mathbf{k}$. The number of initial states between these two energies, $N(E,\hbar\omega)dE$, will be proportional to the square of the matrix element and to dA. We therefore obtain the expression for the energy distribution of photoexcited electrons:

$$P(E,\hbar\omega)=\text{const}\times|V_G/\hbar\omega|^2, \quad E_{\min}<E<E_F$$
$$=0, \quad \text{elsewhere}.$$

The leading peak is therefore expected to be rectangular in shape. This is at variance with the experimental results, which show a triangular shape. It remains to be seen whether this is due to lack of experimental resolution or to inadequacies in the simple theory. The height of the peak is expected to vary with frequency according to ω^{-2}. The peaks shown in Figs. 4–9 do indeed decrease sharply in height with increasing frequency. An exact comparison is difficult to make, however, since $P(E,\hbar\omega)$ is the energy distribution of photo*excited* electrons per *absorbed* photon, whereas the EDC is the energy distribution of photo*emitted* electrons per *incident* photon. To obtain a theoretical prediction of the latter, we would have to introduce the $(1-R)$ and escape factors discussed in Sec. III. We merely point out that the systematics of the width and height-leading peak with changing frequency are in tolerable agreement with nearly free-electron theory, even though we are unsuccessful in predicting its exact shape.

Incidentally, we note that the total area of the disk of permitted initial states is $\pi(m/\hbar G)^2(\omega_{\rm hi}-\omega)(\omega-\omega_{\rm lo})$. Summing over the whole set of $\langle 110\rangle$ reciprocal-lattice vectors, leads to the well-known Wilson-Butcher[29,30] expression for the optical absorption,

$$\omega^2\epsilon_2=\frac{4me^2|V_{110}|^2}{\hbar^4G_{110}\omega^2}(\omega_{\rm hi}-\omega)(\omega-\omega_{\rm lo}), \quad \omega_{\rm lo}<\omega<\omega_{\rm hi}$$
$$=0, \quad \text{elsewhere}.$$

The measurements of ϵ_2 by Smith[3] are in agreement, at least qualitatively, with this nearly free-electron pre-

[29] A. H. Wilson, *The Theory of Metals* (Cambridge University Press, New York, 1936), p. 133.
[30] P. N. Butcher, Proc. Phys. Soc. (London) **A64**, 50 (1951).

diction. To this extent, the optical and photoemission data are in mutual accord.

VI. SCATTERING BY ELECTRON-ELECTRON INTERACTIONS

The electron-electron interaction can influence photoemission properties in two ways. First, the scattering length or mean free path $l(E)$, due to electron-electron interactions, decreases rapidly with increasing excitation energy, and can drop below 10 Å. The mean free path for electron-phonon interactions estimated from the dc conductivity is ~400 Å. The scattering due to electron-electron interactions dominates; moreover, it is inelastic. The scattering length enters directly into the expression for the EDC through the arrival factor $\alpha l(1+\alpha l)$, introduced in Sec. III. Second, electrons which have undergone an inelastic scattering may still be sufficiently energetic to escape from the metal, and thus give rise to a contribution of slow secondary electrons in the EDC. We will consider each of these effects separately.

A. Scattering Length $l(E)$

An excited electron interacts with the electrons inside the Fermi sea and may decay either by creation of a particle-hole pair, or, if its energy is in excess of $E_F+\hbar\omega_p$, by creation of a plasmon. The mean free path for plasmon creation has been derived theoretically by Thomas[5] and by Quinn,[7] and is given by

$$l_{\rm plas}(E)=2a_B\frac{E}{\hbar\omega_p}\left(\ln\frac{(1+y_p)^{1/2}-1}{x-(x^2-y_p)^{1/2}}\right)^{-1}, \quad E>E_F+\hbar\omega_p \qquad (6.1)$$
$$=\infty\,, \quad E\leq E_F+\hbar\omega_p.$$

Here, E is measured from the bottom of the free-electron band, $\hbar\omega_p$ is the plasmon energy, $y_p=\hbar\omega_p/E_F$, $x=(E/E_F)^{1/2}$, and $a_B=0.529$ Å, the Bohr radius. Thomas[5] indicates that plasmon creation is the dominant process, in which case we would expect from Eq. (6.1) to see a dramatic singularity in $l(E)$ on passing through the energy $E_F+\hbar\omega_p$. Such a singularity would be readily apparent in the EDC since the escape probability of an electron excited to energy E involves the factor $\alpha l/(1+\alpha l)$. We would expect the high-energy end of the EDC to be severely attenuated starting from $E=E_F+\hbar\omega_p$. Reference to Figs. 6–11 shows that nothing particular happens in the EDC's at this energy. We offer the following arguments to account for this.

A reliable analytic expression for the particle-hole pair contribution to the scattering is more difficult to obtain. Quinn's[7] approximate formula for the self-energy of a quasiparticle just above the Fermi level may be converted to the following expression for the mean free path due to pair creation:

$$l_{\rm pair}(E)\approx(a_BK/y_p)[x^2/(x^2-1)^2], \qquad (6.2)$$

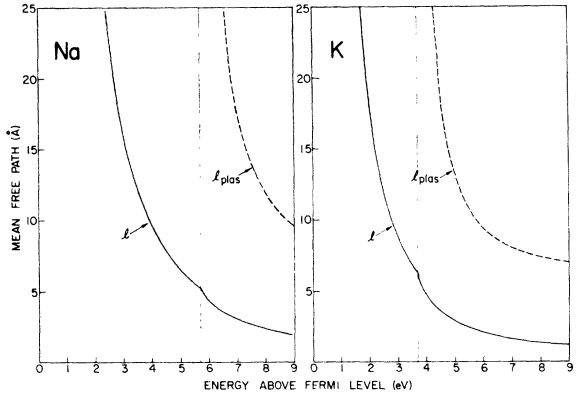

FIG. 15. Calculated mean free paths due to electron-electron interactions in both Na and K. Broken curves labeled $l_{\rm plas}$ are mean free paths due to plasmon creation alone. Curves labeled l include both plasmon and pair creation.

where

$$K=(512/3)\beta^3[\arctan(1/\beta)+\beta/(1+\beta^2)]$$

and

$$\beta=[(4\pi/9)^{1/3}r_s]^{1/2}$$

and where a_Br_s is the radius of a sphere whose volume equals the volume per electron. The combined mean free path is then given by

$$l(E)=l_{\rm pair}l_{\rm plas}/(l_{\rm pair}+l_{\rm plas}). \qquad (6.3)$$

Numerical values obtained for l and $l_{\rm plas}$ are plotted against energy for both Na and K in Fig. 15. First of all, we note that these calculated mean free paths are extremely short. If the photoelectrons have originated from the first few atomic layers, this might raise doubts as to the validity of a volume approach. However, the formulas above are only approximate; it may be unwise to attach too much significance to the actual numerical values at this time. For example, Eq. (6.2) only strictly applies in the immediate vicinity of the Fermi level, and will grossly underestimate $l_{\rm pair}$ for energies more than 1 eV or so above E_F. We merely point out that scattering due to pair creation is not negligible and that when it is included, the variation of $l(E)$ on passing through $E=E_F+\hbar\omega_p$ is not as dramatic as when plasmon scattering is considered alone. Nevertheless, Fig. 15 shows that $l(E)$ still has a pronounced discontinuity in slope at $E=E_F+\hbar\omega_p$. We now argue that even this feature is probably unreal due to the phenomenon of plasmon damping.

The existence of the discontinuity of slope of $l(E)$ hinges on the assumption that the spectrum of elementary excitations can be completely separated into plasmons and particle-hole pairs. However, it is well known[31] that even in the long-wavelength limit, the possibility of interband transitions acts to broaden the plasmon peak in the energy-loss function. The momentum transfers in the scattering processes considered

[31] D. Pines, as in Ref. 14, p. 177.

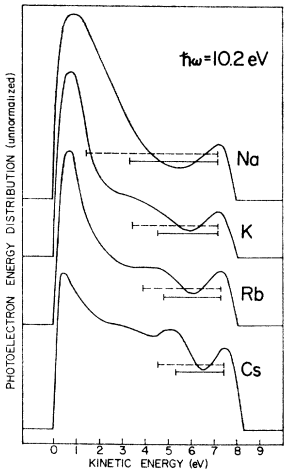

FIG. 16. Photoelectron energy distributions at $\hbar\omega = 10.2$ eV for Na, K, Rb, and Cs. Full horizontal lines represent surface plasmon energies. Broken horizontal lines represent volume plasmon energies.

here are well removed from the long-wavelength limit. For example, the minimum momentum transfer required for an electron to decay from the energy sphere at $E_F + \hbar\omega_p$ to the energy sphere at E_F is $\sim 0.7k_F$ for both Na and K. This is quite close to the Bohm-Pines critical momentum, which is $\sim 0.9k_F$ for both Na and K. For these large momenta, the dispersion of the plasma frequency will be appreciable, and Nozierès and Pines[32] indicate that multipair excitations will be becoming important. All these effects will combine to broaden the plasmon energy loss, and will therefore smooth away the discontinuity in slope of $l(E)$, serving to explain the absence of corresponding structure in the EDC's.

B. Secondary Electrons

Electrons which have suffered an inelastic scattering process may still appear in the energy distributions, but at lower energies. The abundance of such secondary electrons is one of the major features of our experimental EDC's. The distribution of the secondaries may be regarded as the energy-loss spectrum for hot electrons, in close analogy with characteristic loss spectra which have been extensively measured for very fast electrons.[14] It is therefore of some interest to see if we can identify either of the two basic loss mechanisms, pair creation or plasmon creation, in the experimental data.

The low-energy peak about 1 eV above the vacuum level which appears in both the Na and K data (see Figs. 8 and 11) can be understood in terms of loss by pair creation. An approximate approach due to Berglund and Spicer predicts energy-loss spectra of this shape showing a peak just above threshold. The really intriguing question, however, concerns the origin of the broad intermediate piece of structure which appears in K between the leading peak and the low-energy peak (see Fig. 11). One possibility, based on the pair-creation approach, is that this intermediate bump represents the once-scattered electrons, while the low-energy peak represents the twice-scattered and multiply scattered electrons. Eastman[33] has had a certain amount of quantitative success with such an interpretation using the Berglund-Spicer approach.

Another possibility for the intermediate peak in K is that it is due to a discrete loss by plasmon creation. The systematic trends as one proceeds across the alkali-metal series tend to support this explanation. In Fig. 16 we show the EDC's taken at $\hbar\omega = 10.2$ eV for Na and K together with preliminary curves taken recently[34] on Rb and Cs. On each curve we indicate the magnitudes of the surface and volume plasmon energies, determined from characteristic energy-loss experiments by Kunz.[10] Na has the largest plasma frequency and no intermediate bump can be discerned. If it exists, it is presumably still buried in the low-energy peak. In this connection, we note that the low-energy peak is much wider for Na than in the other metals. In Rb, the bump is more pronounced and closer to the leading peak than in K, a trend which continues into Cs. The systematic trends are therefore consistent with the changes in plasmon energy. In Rb and Cs the intermediate peak is sufficiently pronounced to enable us to make a reliable measure of its energy separation from the leading peak. It can be seen in Fig. 16 that the energy separation in these metals is closer to the surface plasmon energy than the volume plasmon energy. Callcott and Mac Rae[35] have observed discrete energy losses in heavily cesiated samples of Ni which they indentify as volume plasmons in the Cs. Energy-loss measurements by Mac Rae *et al.*[36] on cesiated W, on the other hand, show discrete losses due to surface plasmons associated with the Cs. These latter experiments appear to be more consistent with our own work.

It is to be noted that the structure which we attribute to plasmon creation is superimposed on a large background which we have attributed to pair creation. Rough estimates of the relative proportions based on an inspection of Figs. 11 and 16 indicate that pair creation appears to be as important if not more important than plasmon creation. There is some theoretical reason for expecting such behavior. The momentum transfers involved in the scattering processes considered here are quite large, so that pair creation and even multipair creation are quite strong. The sum rule on the energy-loss function requires the plasmon creation must become relatively weaker.

VII. SUMMARY OF CONCLUSIONS

Our attempt to interpret our measurements of the photoemission properties of Na and K in terms of the

[32] D. Pines and P. Nozières, *Theory of Quantum Liquids* (W. A. Benjamin, Inc., New York, 1966), Vol. I, p. 226.

[33] D. E. Eastman (private communication).
[34] N. V. Smith and G. B. Fisher (to be published).
[35] T. A. Callcott and A. U. Mac Rae, Phys. Rev. **178**, 966 (1969).
[36] A. U. Mac Rae, K. Müller, J. J. Lander, J. Morrison, and J. C. Phillips, Phys. Rev. Letters **22**, 1048 (1969).

prevailing three-step picture of the photoemission process has been reasonably successful. In this picture, the three stages, (1) optical excitation of electrons, (2) transport of some of these electrons to the surface, and (3) escape of some of these electrons across the surface, are considered to occur independently.

The measured photoelectric yield per incident photon was found to have a peak just below the plasma frequency and then drop sharply on passing through the plasma frequency. The simple model predicts that the yield per incident photon should be proportional to $(1-R)\alpha$. Values of $(1-R)\alpha$ obtained from the measured optical constants below 4 eV and plausible extrapolations above 4 eV showed the peaking effect and drop on passing through the plasma frequency similar to those in the yield. Our conclusion is that the variation of the yield can be understood in terms of the optical constants and the three-step model. We note that it was not necessary to invoke any sudden variation in the energy dependence of the mean free path.

The energy distributions of photoemitted electrons revealed a peak at the high-energy end which, in the three-step model, we identify as primary or unscattered electrons. The width of this peak was found to decrease with decreasing photon energy, an effect which can be understood in terms of the direct (i.e., **k**-conserving) nature of the optical excitation. A simple theory of direct transitions within the nearly free-electron model is able to explain the systematics of the width and height of the leading peak, but not its observed shape. The predicted shape is rectangular, whereas the observed shape is triangular. It remains to be seen whether this is due to an outright failure of the theory or the need to include extra effects such as lifetime broadening.

The region of the EDC's below the leading peak presents a kind of characteristic energy-loss spectrum. An intermediate piece of structure is observed in the EDC's for K, which we identify as a plasmon energy loss. This intermediate peak cannot be clearly discerned in Na, but is seen in our preliminary data on Rb and Cs, becoming progressively more pronounced and closer to the leading peak. These systematic trends are consistent with a plasmon interpretation. The separation of the intermediate peak and the leading peak in the latter metals leads us to prefer a surface, rather than a volume, plasmon loss.

Although we have interpreted our data solely in terms of the conventional three-step picture of the photoemission process, other possibilities cannot be ruled out. In fact, the very low values estimated for the electron-electron scattering length indicate that many-body effects are quite important. If so, it might be more appropriate to include the electron-electron scattering in the optical excitation process, as suggested by Nesbet and Grant[16] and by Sutton and Hopfield,[15] or in the setting up of the electronic states as done by Hedin, Lundqvist, and Lundqvist.[17] The similarity between the low-energy structure in the electron energy distribution predicted by the latter authors and the intermediate bump which we observe in the EDC's for K is particularly striking. However, it appears that this theory would require modification to accommodate surface plasmons in addition to volume plasmons.

ACKNOWLEDGMENTS

We would like to thank Galen B. Fisher for his help in analyzing the experimental data, and J. MacGowan and S. Wanner for their skilled work in constructing apparatus. We are grateful also for interesting discussions with Professor J. J. Hopfield and Leon Sutton, and our colleagues at Stanford.

PHYSICAL REVIEW VOLUME 188, NUMBER 2 10 DECEMBER 1969

Hyperfine Fields of Technetium and Zinc Impurities in Iron

P. INIA, Y. K. AGARWAL,* AND H. DE WAARD
Natuurkundig Laboratorium der Rijksuniversiteit, Groningen, The Netherlands
(Received 16 July 1969)

The magnetic hyperfine fields of technetium and zinc impurities in an iron lattice have been measured by perturbed angular correlation methods. The fields were found to be -400 ± 160 kOe for Tc in Fe and -105 ± 35 kOe for Zn in Fe. The accuracy is determined by that of the g factor of the intermediate state. The results fit well between the known values of the hyperfine fields of neighboring nuclei in iron.

I. INTRODUCTION

LARGE magnetic fields are often found at nuclei of nonmagnetic elements when these nuclei are embedded as dilute impurities in ferromagnetic metals.[1] These fields are of interest both for nuclear physics and for solid-state physics. Extensive use of these fields has been made in measuring the magnetic moments of

* On leave from Tata Institute of Fundamental Research, Bombay.

[1] B. N. Samoilov, V. V. Sklyarevskii, and E. P. Stephanov, Zh. Eksperim. i Teor. Fiz. **36**, 644 (1959) [English transl.: Soviet Phys.—JETP **36**, 448 (1959)].